Springer

KSME

Journal of Mechanical Science and Technology 24 (12) (2010) 2597~2604
www.springerlink.com/content/1738-494x
DOI 10.1007/s12206-010-0915-1

3-D Simulation of the combustion process for di-methyl ether-fueled diesel engine †

Jaeman Lim[1], Yongrae Kim[1], Sangyul Lee[1], Jaewoo Chung[2], Woo Kang[2] and Kyoungdoug Min[1,*]

[1]*School of Mechanical and Aerospace Engineering, Seoul National University, Seoul, 151-742, Korea*
[2]*Korea Automotive Technology Institute, 74 Yongjung-li Pungse-myun Chunan Choongnam, 330-912, Korea*

(Manuscript Received March 4, 2010; Revised June 1, 2010; Accepted July 29, 2010)

Abstract

The characteristics of spray, auto-ignition, and the combustion process of di-methyl ether(DME) were investigated using a 3-D simulation of a combustion vessel under various engine conditions, including high temperature and pressure. Spray impingement and non-premixed combustion models were incorporated into the computational fluid dynamics code, called STAR-CD. A Peng-Robinson equation of state was introduced to calculate the evaporation rate of DME droplets that were exposed to high-pressure conditions. A Laminar flamelet concept was used to simulate non-premixed combustion. A skeletal chemical kinetics mechanism consisting of 28 species and 45 reactions was used as the chemical mechanism for DME. Compared with the experimental data, the flamelet concept combustion model predicted the essential features of the combustion process and auto-ignition characteristics of the DME spray reasonably well for various initial conditions. The combustion process of a direct injection engine fueled by DME was also simulated and verified through experimental data.

Keywords: 3-D CFD code; Flamelet model; Non-premixed combustion; NOx emissions; Reduced chemical kinetic mechanism

1. Introduction

Combustion processes and alternative fuels for diesel engines intended for reducing NOx and PM emissions have been the focus of recent investigations. Lately, DME (Dimethyl ether-CH3OCH3) has attracted considerable attention as an alternative fuel due to its high vapor pressure, low viscosity, and high cetane number [1], all of which minimize PM and NOx emissions. DME has a cetane number of approximately 60 which is very similar to that of conventional diesel fuel. The PM emission level of DME-fueled diesel engines is significantly lower due to the oxygen content of DME. This reduction in PM emission has led many researchers to study DME engines as a smokeless, clean fuel alternative to diesel vehicles. For instance, Kajitani et al. tested a DME fueled engine and reported that its thermal efficiency was as good as that of a diesel engine [2]. Wakai et al. studied the ignition delay of the DME fuel under high pressure and temperature conditions [3]. Meanwhile, Tsutsumi et al. conducted research on HCCI combustion characteristics using DME for fuel [4]. Tsuchiya and Sato [5] developed a commercial DME engine for use in a heavy-duty truck and then performed various experiments on its performance and emissions.

DME differs from diesel fuel in many ways, most notable of which is the fact that DME is a gas under normal atmospheric conditions. Due to a lower saturated vapor pressure, the penetration length and angle of a DME spray are different from those found in a diesel spray. Although its cetane number is similar, the ignition delay of a DME spray is shorter than that of a diesel fuel spray because it has a shorter mixing time. The amount of fuel injected in each cycle must be reconsidered because the liquid density and specific energy content of DME are about 80% and 70%, respectively, those of diesel fuels.

For the aforementioned reason, the diesel engine needs to be modified to perform optimally while using DME fuel [6]. The development of a computational tool describing the combustion phenomena of the DME spray is useful in making efficient engine modifications. There exist several papers concerned with computational simulations of the combustion of DME spray. For example, Teng et al. [7] calculated the thermodynamic properties of DME fuel in both liquid and vapor phases. Curran et al. [8] developed a detailed chemical kinetic mechanism for DME fuel that consisted of 78 species and 356 reactions. On the other hand, Kim et al. [9] simplified that mechanism to 28 species and 45 reactions. Furthermore, Salsing et al.

† This paper was recommended for publication in revised form by Associate Editor Ohchae Kwon
* Corresponding author. Tel.: +82 2 880 1661, Fax.: +82 2 880 1661
E-mail address: kdmin@snu.ac.kr

[10] used a PaSR combustion model to simulate the performance and emission of a DME engine using a detailed chemical mechanism. Yet, despite their efforts, no synthesis study about DME fuel concerning vaporization, auto-ignition, or combustion of spray using CFD simulation exists.

In this study, a systematic examination of the DME spray and of the combustion process of a DME-fueled engine was performed. A new high-pressure vaporization model was developed to simulate the liquid and vapor spray length of a DME spray at high pressure and temperature conditions. A multiple flamelet combustion model was applied to investigate the combustion characteristics of the DME spray and to estimate the ignition delay time. Finally, the combustion process of a diesel engine fueled by DME was simulated and verified through experimental data.

2. Modeling

2.1 Spray breakup model

The calculation of the spray characteristics was performed using a commercial CFD code-STAR-CD [11]. The breakup model proposed by Reitz and Diwakar [12] was used to simulate the droplet breakup process, with the model coefficients adjusted specifically for a DME liquid. The model of O'Rourke [13] was used as a collision model and coalescence among droplets. The measured DME injection rate was also used in this simulation.

2.2 High pressure vaporization model

In classical vaporization models, the evaporation rate of droplets can be calculated using the Clausius-Clapeyron equation [14], which is based on the ideal gas equation of state. However, the assumption of an ideal gas may not be valid in a high-pressure environment, especially for a fuel that has a low boiling temperature, such as DME. The Peng-Robinson EOS (Equation of State) [15] was introduced in this study to calculate the fugacity and the mass fraction of the vapor at the droplet surface. The Peng-Robinson EOS is expressed as follows:

$$P = \frac{\bar{R}T}{v - b} - \frac{a(T)}{v(v+b) + b(v - b)} \tag{1}$$

where b and a(T) are equation coefficients. The partial molar fugacity for the component i in the mixture was deduced using the Peng-Robinson EOS expressed by:

$$ln\left(\phi_i\right) = \frac{b_i}{b\bar{R}T}\left(Pv - \bar{R}T\right) - ln\left(\frac{P}{\bar{R}T}\left(v - b\right)\right) = \left(\frac{a}{2\sqrt{2}\bar{R}T}\right)\left(\frac{2\sum_{j=1}^{N} x_j a_{ij}}{a} - \frac{b_i}{b}\right) ln\left(\frac{v+(1+\sqrt{2})b}{v+(1-\sqrt{2})b}\right). \tag{2}$$

The condition for thermodynamic equilibrium is dGt,p=0 , which is equivalent to the following:

$$x_{fuel}\phi_{fuel}{}^{L} = y_{fuel}\phi_{fuel}{}^{V}, x_{air}\phi_{air}{}^{L} = y_{air}\phi_{air}{}^{V}. \tag{3}$$

Using this information, the mixture fraction of the vapor at the droplet surface Y_s was calculated [16]. The evaporation rate can be predicted using the standard Spalding equation stated as [15]:

$$\dot{m}_d = 2\pi r\rho D_{AB} ln(B+1)(2.0 + 0.533 Re_d^{1/2} Pr_d^{1/3}) \qquad B = \frac{Y_{f,s} - Y_{f,\infty}}{1 - Y_{f,s}}. \tag{4}$$

In the above, ρ is the density of background air, D_{AB} is the diffusivity between droplet and air, and $Y_{f,\infty}$ is the fuel mixture fraction of the background air.

The heat transfer coefficient was ascertained using the formula by Wakal [16] expressed by:

$$h = \frac{k_g NuZ}{\left(e^Z - 1\right)D_d}, \quad Z = \frac{-c_P\left(dm_d/dt\right)}{\pi D_d k_g Nu}. \tag{5}$$

In the above, k_g is the thermal conductivity and c_p is the specific heat of the mixture.

2.3 Reduced chemical kinetic modeling

A reduced chemical kinetic mechanism proposed by Kim et al. [9] was used to deduce the detailed chemical kinetic mechanism of DME, which consisted of 336 chemical reactions and 78 chemical species [8]. This has reduced chemical kinetic mechanism consisting of 45 reactions and 28 species as presented in Table 1. The first 20 reactions are in the low temperature NTC regions, whereas the other reactions are in the high temperature region. The schematic diagram for the overall reaction path of DME oxidation is presented in Fig. 1.

To calculate the ignition delay from the reduced chemical kinetic mechanism, we considered both the species equation and the energy equation. The reacting mixture was then treated as a closed system with no mass crossing the system boundary, of which the total mass of the mixture remained constant.

2.4 Flamelet combustion model

There are many types of combustion models that can predict the combustion characteristics of the diffusion flame; however, most of these models require the input of empirical parameters that cannot be determined without conducting an experiment. In order to predict the performance of an engine in the design stage, a combustion model without empirical factors is thus needed.

Peters [17] introduced the concept of a laminar diffusion flamelet residing in the vicinity of the surface where a sufficiently high local mixture gradient exists. He introduced a coordinate system, which is that is attached to the surface of

Table 1. Reduced chemical kinetic mechanism for DME.

1. $CH_3OCH_3 + O_2 = CH_3OCH_2 + HO_2$
2. $CH_3OCH_2 + O_2 = CH_3OCH_2O_2$
3. $CH_3OCH_2O_2 = CH_2OCH_2O_2H$
4. $CH_2OCH_2O_2H + O2 = O_2CH_2OCH_2O_2H$
5. $O_2CH_2OCH_2O_2H = OCH2OCHO2H + OH$
6. $OCH_2OCHO_2H = OCH_2OCHO + OH$
7. $CH_3OCH_3 + OH = CH_3OCH_2 + H_2O$
8. $CH_3OCH_2 + O_2 = HO_2 + CH_2O + CH_2$
9. $HO_2 + HO_2 = HOOH + O_2$
10. $HOOH + M = OH + OH + M$
11. $CH_3OCH_2O_2 + HO_2 = CH_3OCH_2O_2H + O_2$
12. $CH_2OCH_2O_2H = CH_2O + CH_2O + OH$
13. $OCH_2OCHO = HOCH_2OCO$
14. $OCH_2OCHO = CH_2O + HCO_2$
15. $CH_3OCH_2O_2H = CH_3OCH_2O + OH$
16. $CH_3OCH_3 + CH_3OCH_2O_2 = CH_3OCH_2 + CH_3OCH_2O_2H$
17. $CH_3OCH_3 + HO_2 = CH_3OCH_2 + HOOH$
18. $CH_3OCH_3 = CH_3 + CH_3O$
19. $CH_3OCH_2O = CH_3O + CH_2O$
20. $HOCH_2OCO = CH_2OH + CO_2$
21. $OH + OH = HO_2 + H$
22. $H + O_2 + M = HO_2 + M$
24. $OH + H + M = H2O + M$
25. $O + O + M = O2 + M$
26. $CO + OH = CO2 + H$
27. $CO + HO2 = CO2 + OH$
28. $CO + O + M = CO2 + M$
29. $CO + O2 = CO2 + O$
30. $H + O2 = O + OH$
31. $HCO + O2 = CO + HO2$
32. $HCO + OH = CO + H2O$
33. $HCO + O = CO2 + H$
34. $HCO + M = CO + H + M$
35. $CH_3 + O_2 = CH_2O + OH$
36. $CH_3 + O_2 = CH_3O + O$
37. $CH_3 + HO_2 = CH3O + OH$
38. $CH_2 + O_2 = HCO + OH$
39. $CH_3O + O_2 = CH_2O + HO_2$
40. $CH_3O + M = CH_2O + H + M$
41. $CH_2OH + O_2 = CH_2O + HO_2$
42. $CH_2O + OH = HCO + H_2O$
43. $CH_2O + O = HCO + OH$
44. $CH_2O + HO_2 = HCO + HOOH$
45. $CH_2O + O_2 = HCO + HO_2$

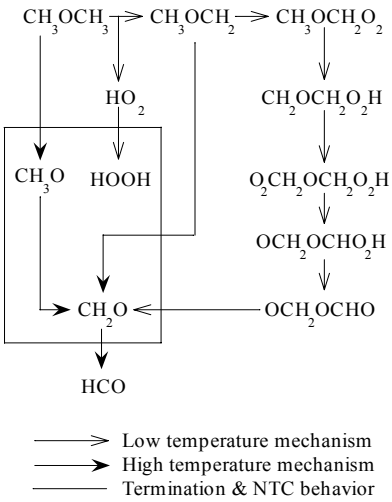

Fig. 1. Schematic diagram of the overall reaction path of DME oxidation.

the stoichiometric mixture and deduced the unsteady 2nd order partial differential equations about the temperature and species expressed by:

$$\rho\frac{\partial Y_i}{\partial t} = \frac{\rho\chi}{2}\frac{\partial^2 Y_i}{\partial Z^2} + \dot{m}_i \quad \text{and} \tag{6}$$

$$\rho\frac{\partial T}{\partial Z} = \frac{\rho\chi}{2}\frac{\partial^2 T}{\partial Z^2} + \frac{\rho\chi}{2}\frac{1}{c_p}\frac{\partial c_p}{\partial Z}\frac{\partial T}{\partial Z} - \frac{\rho\chi}{2}\frac{\partial T}{\partial Z}\sum_{k=1}^{N}\frac{c_{p,k}}{c_p}\frac{\partial Y_k}{\partial Z} - \frac{1}{c_p}\left(\sum_{k=1}^{N}h_k\dot{m}_k - \frac{\partial p}{\partial t}\right), \tag{7}$$

where Y_i is the species concentration, $\dot{m}$ is the change of species from chemical reactions, T is the temperature, Z is the mixture fraction, h is the enthalpy, and p is the pressure.

In these equations, the parameter χ is designated as the scalar dissipation rate. It has a dimension of one unit per second and may be interpreted as the inverse of the characteristic diffusion time. This factor represents the instantaneous local diffusion and the strain effects due to the flow field. As the factor increases, heat transfer from the reaction zone to the surrounding inertia induces an effect, which causes an increase in the ignition delay. The χ–profile for a small mixture fraction in the configuration of counter-flow geometry can be modeled as [19]:

$$\chi = 4a_s Z^2 [erfc^{-1}(2Z)]^2 = 4a_s f(Z) \tag{8}$$

The turbulent diffusion flame can be treated as an ensemble of laminar diffusion flamelets and can be averaged by the Probability Density Function (PDF). The unconditional mean scalar dissipation rate can be modeled as follows:

$$\tilde{\chi} = c_x\frac{\tilde{\varepsilon}}{\tilde{k}}\widetilde{Z''^2} \tag{9}$$

The conditional Favre mean scalar dissipation rate can be expressed as [18]:

$$\tilde{\chi}_{st} = \frac{\tilde{\chi} f(Z_{st})}{\int_0^1 f(Z)\tilde{P}(Z)dZ} \tag{10}$$

The averaged value of this parameter was then used in both Eqs. (6) and (7).

This method does not require empirical parameters and can separate numerically the chemical time scale from the turbulent time scale. The procedure detailed below can be used to analyze the combustion phenomena using a detailed chemical kinetic mechanism:

- At each step, the CFD code calculates the distribution of the mixture fraction, the boundary conditions, and the scalar dissipation rate of the combustion field at each step.
- From the CFD code, the flamelet code calculates the species and temperature distributions in the mixture fraction coordinate. This calculation is performed using a much shorter time step than what is used in the CFD code. The results are then delivered to the CFD code in the Favre-averaged form found in the turbulent flow. Using these results, the CFD code calculates the temperature of each cell.
- The Chemkin library delivers the enthalpy of each cell to the CFD code, and the reaction rate to the flamelet code.

The relationships among the CFD code, Flamelet code, and Chemkin library are summarized in Fig. 2. These procedures were used in various papers in simulating the combustion process of a diesel engine during normal injection conditions as shown in example [20].

2.5 Multiple flamelet

The scalar dissipation rate represents the turbulent characteristics in the combustion field [17]. The scalar dissipation rate varies spatially as injection progresses. In order to accurately simulate the auto-ignition site and ignition delay, this spatial variation in the scalar dissipation rate must then be considered.

Different marker particles that were taken from the turbulent flow field, were introduced in order to consider different flamelet histories [19]. The transport equation that gives the probability of finding a marker particle is expressed by:

$$\frac{\partial \bar{\rho}\tilde{I}_l}{\partial t} + \nabla\cdot(\bar{\rho}\tilde{\mathbf{v}}\tilde{I}_l) - \nabla\cdot\left(\bar{\rho}\frac{\upsilon_T}{Sc_T}\nabla\tilde{I}_l\right) = 0\,. \tag{11}$$

These parameters represent the contribution of each flamelet history to the combustion field in the calculation domain. Each species and scalar dissipation rate can be multiplied as follows:

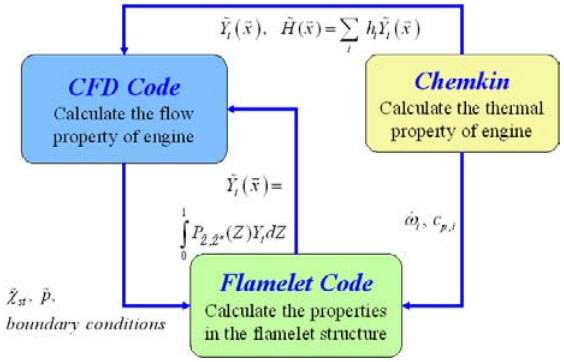

Fig. 2. Schematic diagram of the relationship among the commercial CFD code, flamelet code, and Chemkin library.

$$\tilde{\chi}_{st,overall} = \frac{\sum_{l=1}^{n}\int_V \tilde{I}_l \tilde{\chi}_{st}^{\,3/2}\bar{\rho}\tilde{P}(Z_{st})dV}{\sum_{l=1}^{n}\int_V \tilde{I}_l \tilde{\chi}_{st}^{\,1/2}\bar{\rho}\tilde{P}(Z_{st})dV}\,. \tag{12}$$

3. Results and discussion

3.1 DME spray length in a high temperature and pressure environment

Kim et al. investigated the shape of a DME spray in a constant volume vessel under various high pressure and temperature conditions [9]. The spray was visualized using two methods: the Shadowgraph method, which was used in both the vapor and liquid phases, and the Mie scattering method, which was used for creating liquid phase images. In this study, the spray characteristics under identical conditions were calculated using a commercial CFD code, called the STAR-CD, with sub-models for droplet breakup and evaporation as well as the utilization of the measured DME injection rate throughout the simulation.

To verify the spray and vaporization models used in this study, both liquid and vapor spray lengths for DME were calculated under both high pressure and high temperature conditions and were then compared to the experimental data. The evolution of the DME spray, including both the liquid and vapor phases, is shown in Fig. 3. The nozzle diameter was 0.2 mm, and the ambient pressure and temperature were 30 bar and 600 K, respectively. The simulated results under the same conditions showed an excellent agreement with the experimental images obtained by the shadow graph method. The calculated liquid length increased only by 4 mm after 0.6ms and did not develop to over 24 mm, which was the same result as that obtained in the experiments.

3.2 Auto-ignition and combustion of DME spray

To analyze the characteristics of auto-ignition and combustion, a CFD simulation analysis was performed using STAR-CD. The calculations in this simulation were conducted under high pressure and temperature conditions for a constant vol-

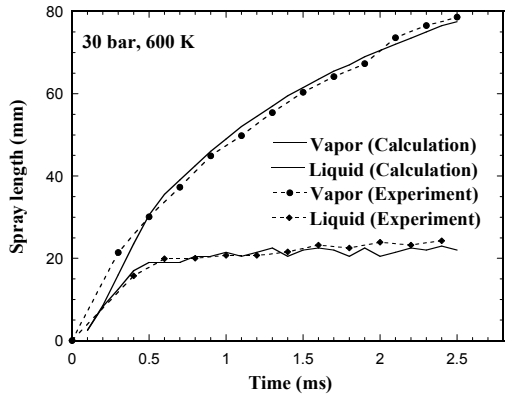

Fig. 3. Comparison of liquid and vapor lengths of DME spray.

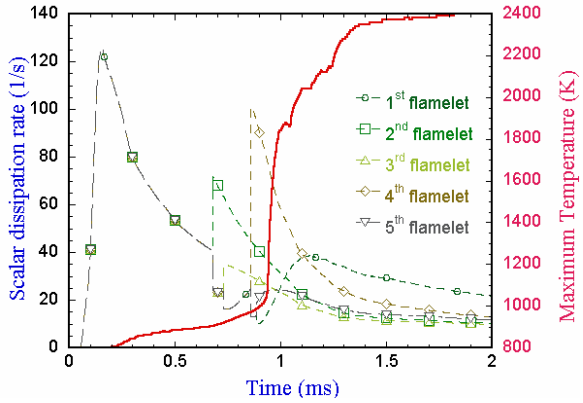

Fig. 4. Time evolution of the local flame structure of temperature in flamelets.

ume vessel, the conditions of which were identical to those used in the experiments. The time evolution of the scalar dissipation rates in this domain is shown in Fig. 4. The initial temperature and pressure were 1,100 K and 21 bar, respectively. The scalar dissipation rate grew to 400 s-1 and, then decreased when injection began. Concerning the evolving mixture field, the spatial variation of the scalar dissipation rate increased. When this variation exceeded a certain limit, the flamelet was subdivided into two at 0.4 ms ASOI (After Start of Injection).

After a period of time, this subdivision was completed successfully, and the scalar dissipation rate of a specific flamelet history decreased below the ignition limit. The temperature at the same part of the domain started to increase at 0.8 ms. At 1.1 ms, the scalar dissipation rate concurrently reached the ignition limit for the first time during the whole flamelet history, after which auto-ignition occurred.

The auto-ignition process of a DME spray can be explained within the mixture fraction domain. In a diffusion flame, high and low temperature regions coexisted and were affected by the turbulent flow. Fig. 5 shows the transient distribution of the concentration of various species and the local temperature. A concentration of HOOH formed at 0.6 ms due to reaction R9, which produced a cool flame in the mixing zone. The

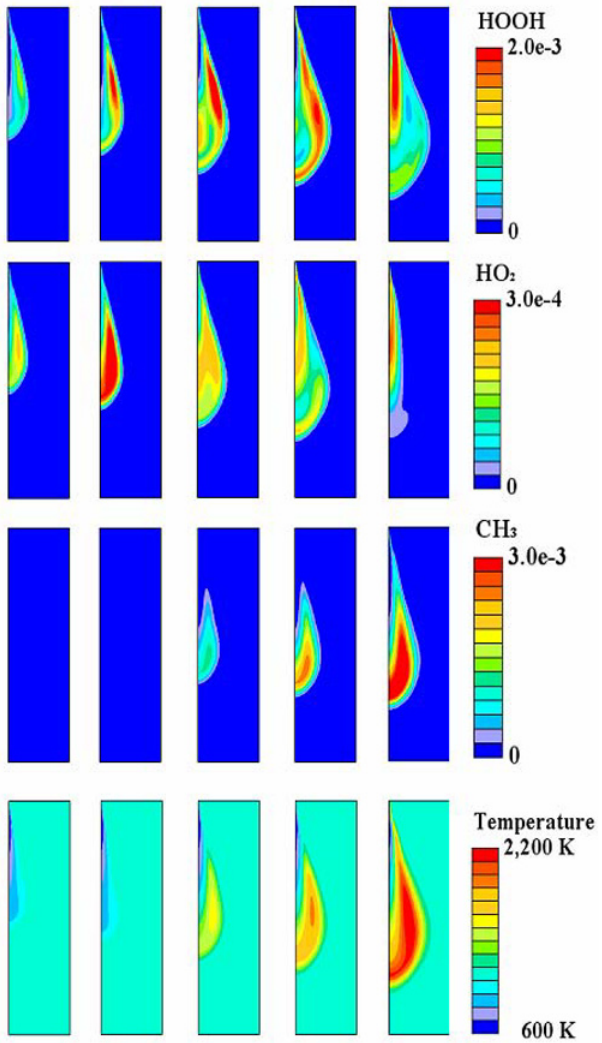

Fig. 5. The spatial distribution of species and temperature of DME spray.

HO_2 radical formed in the stoichiometric field, causing the HOOH radical to be consumed and thereby creating OH through reaction R10, this resulted in an increased temperature of the stoichiometric field. Therefore, after 1.0 ms, the temperature of the stoichiometric field increased to 2,000 K, and the DME decomposed directly into the CH_3 radical due to reaction R19. These reactions did not occur near the injector nozzle because the scalar dissipation rate in this region was too high and the temperature too low.

The calculated and measured ignition delay times under various ambient conditions were compared in Fig. 6. The ignition delay of cases, in which the ambient pressure was 41 bar was calculated to be shorter (by about 1 ms) than that of cases at 21 bar. The combustion model reasonably predicted the auto-ignition delay of the DME spray.

3.3 Engine simulation

A CFD simulation of the DME fueled engine was performed

Table 2. Engine specifications and operating conditions.

Engine Speed (rpm)	2000
Bore x Stroke (mm)	102 x 92
Connecting Rod Length (mm)	167
Compression Ratio	17.4:1
Star of Injection (degree)	10, 15, 20 BTDC
Swirl Ratio	2.0
Nozzle Diameter (mm)	0.4

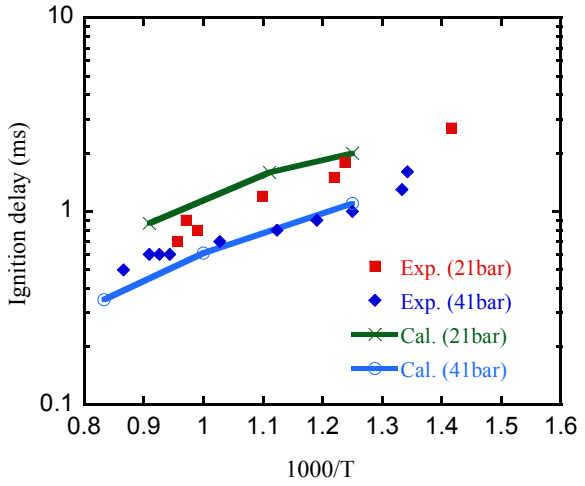

Fig. 6. Experimental and calculated ignition delay times of DME spray under various conditions and comparison with the ignition delay data.

using a moving grid. The computational mesh, consisted of approximately 100,000 cells at BDC and 42,000 cells at TDC, represented 1/6th of the entire combustion chamber. The symmetry of the chamber can be maximized because a six-hole injector was installed. The mesh density was similar to that of the previous work [20]. In order to maintain fine mesh quality during the calculation, the event technique was used to add or remove cell layers in the cylinder liner regions from the piston motion. The piston geometry was of a Mexican-hat type. The details of the engine geometry and the operational conditions used in the simulation are listed in Table 2. The nozzle diameter was 0.5 mm, which was larger than that of the normal diesel injector.

The droplet distributions and temperature contours according to the crank angle are compared in Fig. 7. Auto-ignition occurred at 0◦ ATDC, but the amount of vaporized fuel was very small due to the large droplet size. At 5◦ ATDC, the vaporization and mixing process of droplets were enhanced, and there existed a high temperature region above 2,200 K in the stoichiometric region of the mixture fraction. The high temperature region was developed at 20◦ ATDC to the point of including the whole combustion chamber, although some of the droplets were not yet vaporized. They were instead participating in the combustion phenomena at a slow rate during the expansion stroke. The fuel vapor did not diffuse well to the whole combustion chamber because the large injector diameter produced a rather low speed of injection.

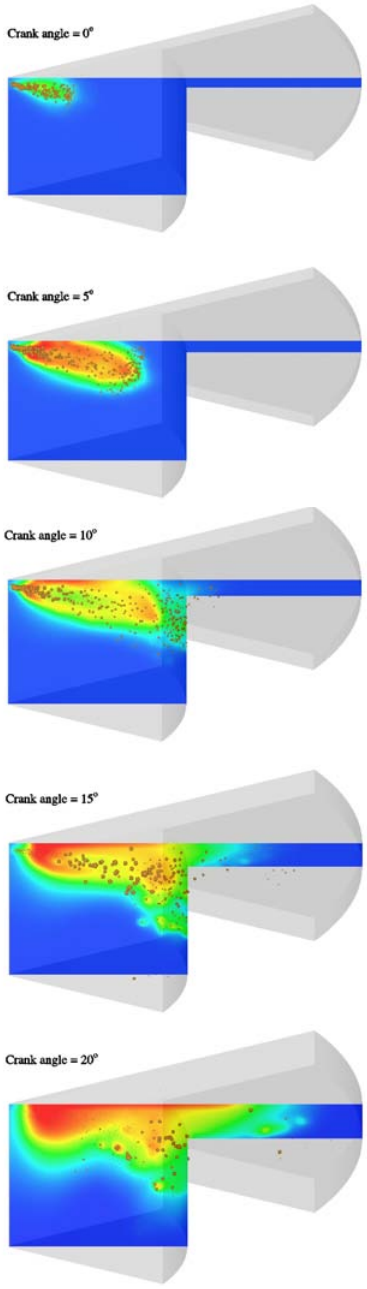

Fig. 7. DME fuel droplet and temperature distribution according to crank angle.

To validate the combustion model used in this study, the cylinder pressure was calculated and compared with the experimental data obtained for various injection timings, as shown in Fig. 8. The tested injection timings were 15◦, 20◦ and 25◦ BTDC. The spray and combustion model used in this paper predicted this phenomenon accurately, and the calculation results agreed well with the experimental data. Due to the rather large size of the injector nozzle, droplet breakup occurred after auto-ignition of the DME fuel. Therefore, the cylinder pressure increased after 0◦ ATDC, where the injected

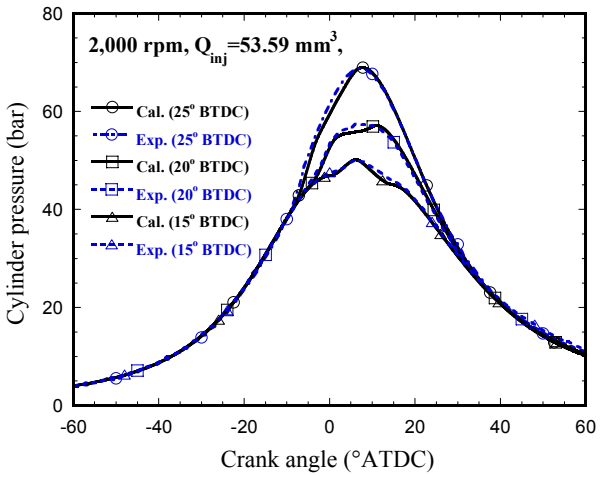

Fig. 8. Comparisons of cylinder pressure of the DME Engine between calculation results and experimental data for two cases.

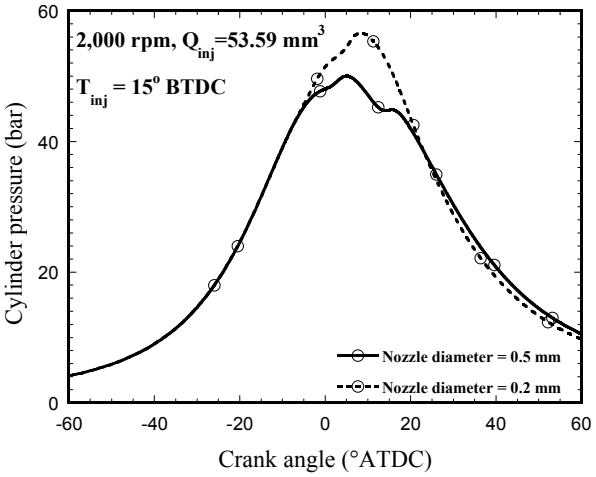

Fig. 9. Comparisons of cylinder pressure of the DME Engine for different injector nozzles.

droplets started to breakup. In the case that the injection timing was 15◦ BTDC, about 10% of the droplets had not vaporized even after 20◦ ATDC. Moreover the rate at which they participated in the combustion phenomena was slow. The maximum pressure was 50 bar at 6◦ ATDC when the injection timing was 15◦ BTDC. The maximum pressure increased when the injection timing was advanced, because more droplets evaporated during the compression stroke. For the cases where the injection timing was 20◦ or 25◦ BTDC, the maximum pressures were 56 bar at 11◦ ATDC and . 69 bar at 6◦ ATDC, respectively.

Due to the long breakup time of the DME droplets in those cases, the engine must be operated under earlier injection timing than that used in a normal diesel engine to obtain an appropriate performance. Thus, engine performance was theorized to improve if the breakup time was faster. The nozzle diameter was reduced to 0.2 mm to observe the effect of breakup time, and the calculation results are compared in Fig. 9. The peak pressure was raised to 71 bar in this case. For this result, the cylinder pressure could be made higher by reducing the nozzle diameter.

4. Conclusions

The development of a DME spray was simulated using the spray model in STAR-CD and the high-pressure vaporization model developed in this work. A 3D simulation using flamelet combustion models was then conducted to calculate the ignition delay time of a DME spray, the results of which were compared to those of the experimental data. Finally, a CFD analysis of a DME engine was performed with a moving grid and compared such analysis to the results from that of a diesel engine. The main findings of the DME spray characteristics and auto-ignition are summarized below.

- The liquid and vapor spray length simulated by STAR-CD during high pressure and temperature conditions showed favorable consistency with the experimental data obtained by spray visualization. The liquid length of the DME spray at a 30 bar and 600 K condition was maintained at 24 mm.
- The flamelet code associated with a commercial CFD code can predict spatial flamelet history, auto-ignition site, and ignition delay of the DME spray reasonably well.
- The CFD simulation of a DME-fueled engine using a moving grid was performed. The calculated cylinder pressure agreed well with the experimental data. In addition, reducing the nozzle diameter enhanced the performance of DME engines because the breakup time of the droplets could be reduced. This simulation tool can be used for engine optimization at the engine design stage.

Acknowledgment

This research was supported (in part) by SNU-IAMD, republic of Korea.

Nomenclature

ASOI : After start of injection
TDC : Top dead center
BDC : Bottom dead center
χ : Scalar dissipation rate (s^{-1})
ρ : Density of gas
Z : Mixture fraction
NTC : Negative temperature coefficient
EOS : Equation of state
PM : Particulate matter
PaSR : Partially stirred reactor
CFD : Computational fluid dynamics

Subscripts

g : Gas phase
d : Droplet

References

[1] S. C. Sorenson and S. E. Mikkelsen, Dimethyl ether as an ignition enhancer for methanol-fueled diesel engines, *SAE Paper No. 912420* (1991).

[2] S. Kajitani, et *al.*, Engine performance and exhaust characteristics of direct–injection diesel engine operated with DME, *SAE Paper No. 972973* (1997).

[3] K. Wakai, K. Nishida, T. Yoshizaki and H. Hiroyasu, Ignition delays of DME and diesel fuel sprays injected by a D.I. diesel injector, *SAE Paper No. 1999-01-3600* (1999).

[4] Y. Tsutsumi, A. Iijima, K. Yoshida, H. Shoji and J. T. Lee, HCCI combustion characteristics during operation on dme and methane fuels, *International Journal of Automotive Technology*, 10 (6) (2009) 645-652.

[5] T. Tsuchiya and Y. Sato, Development of DME engine for heavy-duty truck, *SAE Paper No. 2006-01-0052* (2006).

[6] D. Ushiyama, T. Noda, S. Nozaki and H. Oikawam, An investigation of DME injection characteristics using jerk type In-line injection system, *JSAE 20035068* (2003).

[7] H. Teng, J. C. McCandless and J. B. Schneyer, Thermodynamic properties of dimethyl ether – an alternative fuel for compression-ignition engines, *SAE Paper No. 2004-01-0093* (2004).

[8] H. J. Curran, W. J. Pitz, C. K. Westbrook, P. Dagaut, J-C. Boettner and M. Cathonnet, A Wide Range Modeling study of dimethyl ether oxidation, *Int. J. Chem. Kinet*. 30 (1998) 229-241.

[9] H. Kim, S. Cho and K. Min, Reduced chemical kinetic model of DME for HCCI combustion, *SAE Paper No. 2003-01-1822* (2003).

[10] H. Salsing, C. A. Rinaldini, V. Golovitchev and I. Denbratt, Performance and emissions of DME diesel engine equipped with fuel specific common rail system, *2006 JSAE Annual Congress* (2006).

[11] CD-Adapco, STAR-CD VERSION 3.26 (2005).

[12] R. D. Reitz and R. Diwakar, Effect of drop breakup on fuel spray, *SAE Paper No, 860469* (1986).

[13] P. J. O'Rourke, Collective drop effects on vaporizing liquid sprays, *Ph. D Thesis, Princeton University* (1981).

[14] B. E. Poling, J. M. Praustiz and J. P. O'connel, *The properties of gases and liquids : fifth edition, Mcgraw-Hill* (2001).

[15] D. B. Spalding, The combustion of liquid fuels, fourth symposium (international) on combustion, *The Combustion Institute*, Pittsburge, Penn. (1953).

[16] M. M. El Wakil, O. A. Ueyhara and P. S. Myers, A theoretical investigation of the heating-up period of injected fuel droplets vaporizing in air, *NACA Technical Note 3179* (1954).

[17] N. Peters, Laminar diffusion flamelet models in non-premixed turbulent combustion, *Prog. Energy Combust. Sci.* 10 (1984) 319-339.

[18] N. Peters, Local quenching due to flame stretch and non-premixed turbulent combustion, *Combust. Sci. and Tech.* 30 (1983) 1-17.

[19] N. Peters, *Turbulent combustion, Cambridge University Press* (2000).

[20] H. Barths and N. Peters, Three-dimensional modeling of NOx and soot formation in DI-diesel engines using detailed chemistry based on the interactive flamelet approach, *SAE Paper 962057* (1996).

Jaeman Lim received a B.S. degree in 2000 and a Ph. D. in 2007 in Mechanical Engineering from Seoul National University. Dr. Lim worked as a senior engineer at CD-Adapco Korea from 2007 to 2008 and is currently a senior engineer at the CFD engineer service in CD-Adapco.

Kyoungdoug Min is a Professor at the department of mechanical and aerospace engineering in Seoul National University. He received his B.S and M.S degree in Seoul National University in 1986 and 1988, respectively. Then he graduated with a Ph.D. degree in mechanical Engineering at MIT in 1994. He has worked as a research fellow at Daimler-Benz for 2 years.